

Negative-emission Waste-to-Concrete via Tandem Supercritical Water Oxidation and Hydrothermal Mineralization

David H. Kenney^a, Andrew M. Charlebois^a, Shuai Wang^b, Nima Rahbar^b,

Michael T. Timko^a, Andrew R. Teixeira^{a*}

a) Department of Chemical Engineering, Worcester Polytechnic Institute, Worcester, Massachusetts 01609, United States

b) Department of Civil, Environmental, and Architectural Engineering, Worcester Polytechnic Institute, Worcester, Massachusetts 01609, United States

* Correspondence should be addressed to arteixeira@wpi.edu

Keywords: Bioenergy carbon capture utilization and sequestration (BECCUS), Waste-to-Energy, Green Concrete, CO₂ Oxidation

Table of Contents

1. Results	3
1.1. SCWO of Food Waste to Produce High-Pressure CO ₂	3
Table S1. Chemical and elemental analysis of VA hospital food waste	3
Table S2. Experimental conditions for SCWO reactions	4
Figure S1. Carbon distributions within SCWO products	4
Figure S2. SCWO aqueous phase HPLC analysis	5
Figure S3. SCWO aqueous phase UV-Vis analysis	5
1.2. Rapid and Complete Mineralization of High-Pressure CO ₂	6
Figure S4. Speciation of CO ₂ in aqueous solutions	6
1.3. Carbon Negativity	7
Figure S5. Developed ASPEN/HYSYS model process flow diagram	7
Table S3. Mass and energy balance for 20 wt% solids loading with O:C = 3	8
Figure S6. SCWO energy balances	9
Figure S7. TGA analysis of ACM sample	9
1.4. Material Analysis	10
2. Methods	10
2.1.1. Supercritical Water Oxidation of Food Waste	10

Figure S9. Reaction and analysis diagram	11
Figure S10. Parr reactor vessel used for SCWO experiments	11
Figure S11. GC-TCD calibration curves.....	12
2.1.2. Modeling the SCWO mechanism	12
Table S4. Normalized elemental compositions for dehydrated food waste.....	12
Table S5. Elemental molar ratios within dehydrated food waste.....	13
Figure S12. ODE solution for isothermal SCWO conversion.	14
Figure S13. ODE solution for constant oxidant loading.....	15
2.2. CaCO ₃ yield analysis and kinetic parameters.....	15
Figure S14. XRD calibration of mineralization products.	16
Figure S15. Solution of mineralization rate expression.....	16
2.3. Process Model Development.....	16
2.4. Development of lifecycle analysis.....	18
Figure S16. Process flow diagram for waste-to-concrete process in GREET	18
Figure S17. Process inputs and outputs for SCWO in GREET	19
Figure S18. Process inputs and outputs for calcium hydroxide production.....	20
Figure S19. Process inputs and outputs for calcium brine production.....	20
Figure S20. Process inputs and outputs for ACM production	21
3. References	22

1. Results

1.1. SCWO of Food Waste to Produce High-Pressure CO₂

Food waste obtained from the New Hampshire VA Hospital (Manchester, NH) was selected as a representative wet waste given the availability and abundance of food waste.¹ Food waste characterization data are shown in Table S1. Food waste is typically a highly variable feed as it not only changes seasonally but is also impacted by the source type, region and even socioeconomics of the collection area.² It is typically made up of a high-energy organic fraction (23.6 MJ/kg) primarily consisting of carbohydrates, proteins, and lipids. Compared with green wastes and biosolids, food waste has low-ash content (1.9 wt%) which poses less risk of reactor due to salt precipitation under supercritical water conditions.³

Table S1. Chemical and elemental composition of dehydrated food waste used in this study

Proximate Analysis (wt%)^a	
Moisture	0.7 ± 0.1
Ash	1.9 ± 0.9
Elemental Analysis (wt%)^{a-c}	
Carbon	52.2 ± 0.9
Hydrogen	7.5 ± 0.2
Nitrogen	4.3 ± 0.1
Sulfur	1.0 ± 0.1
Oxygen ^c	33.2 ± 2.1
Biochemical Analysis (wt%)^{a-c}	
Carbohydrates	29.8
Lipids	38.9
Protein ^d	26.8 ± 0.6
Solubility (mg/ml)^f	
	2.4 ± 0.49
HHV (MJ/kg)	
	23.6 ± 3.0

^a Dry Basis

^b As Received

^c Oxygen determined by difference

^d Protein = N-Content × 6.25

^e Standard deviation reported as ±, where n=3

^f Standard deviation reported as ±, where n=2

Table S2. Experimental ratios for each feed component within the supercritical water oxidation experiments

O:C	Food Waste (g)	Water (g)	30 wt% Peroxide Solution (g)	Operating Pressure (atm)
0	1	50	0	211
1	1	46.5	4.9	231
2	1	43.1	9.9	245
3	1	14.8	39.6	265

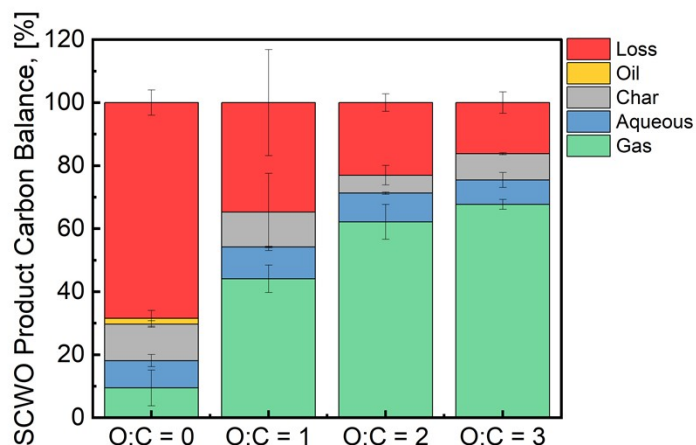


Figure S1. Product carbon distribution for SCWO of solid food waste. Beyond O:C = 0, the oil phase is not recovered in a quantifiable amount. Loss is reduced as the oxidant loading is increased, increasing the amount of CO₂ produced. It is possible that there was a partial oxidation of the carbon causing a co-elution with oxygen/nitrogen which would prevent us from detecting it on the GC.

The HPLC analysis shows a myriad of peaks over the 25-minute analysis. For this study, the compound of interest was acetic acid as it has proven to be a recalcitrant compound in further oxidation steps for SCWO systems. Other small chain carboxylic acids that could be present are: tartaric acid (2 min), protocatechuic (18 min), dihydrobenzoic (19 min) and hydrobenzoic acids (22 min).⁴

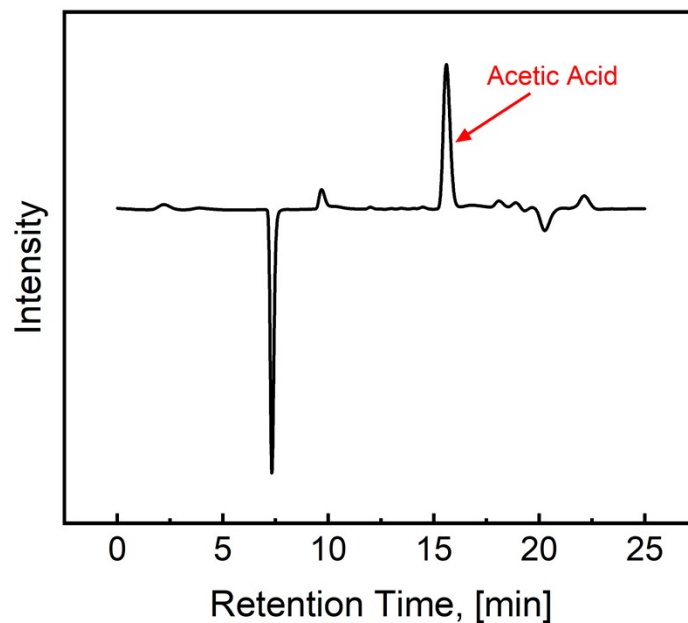


Figure S2. HPLC of aqueous phase identifying acetic acid as one of the primary aqueous products

The UV-Vis analysis of the aqueous phase showed activity in the 220 – 340 range, indicating aromatic compounds.⁵ Based on previous studies and the HPLC analysis in Fig. S2, the activity in this range is likely due to dihydro- and hydroxybenzoic acids.^{6,7}

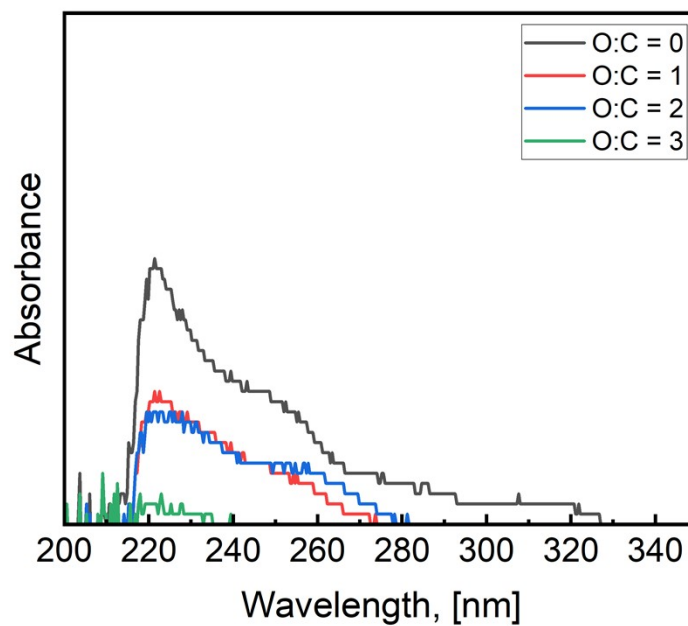


Figure S3. UV-Vis analysis of aqueous phase products after a 1:100 dilution with DI water

1.2. Rapid and Complete Mineralization of High-Pressure CO₂

When dissolved in water, carbon dioxide can form carbonic acid (H₂CO₃) which can dissociate into bicarbonate ions (HCO₃⁻) and then further into carbonate ions (CO₃²⁻). However, this process is heavily dependent on pH as described by the Bjerrum plot equations:

$$x_{CO_2,eq} = \frac{[H^+]_{eq}^2}{[H^+]_{eq}^2 + K_1[H^+]_{eq} + K_1K_2} \quad \#(1)$$

$$x_{HCO_3^-,eq} = \frac{K_1[H^+]_{eq}}{[H^+]_{eq}^2 + K_1[H^+]_{eq} + K_1K_2} \quad \#(2)$$

$$x_{CO_3^{2-},eq} = \frac{K_1K_2}{[H^+]_{eq}^2 + K_1[H^+]_{eq} + K_1K_2} \quad \#(3)$$

Here, K₁ and K₂ are the two acid equilibrium constants associated with carbonic acid, where K₁ is 1.42 · 10⁻⁶ and K₂ is 1.26 · 10⁻⁹.⁸ In Figure S4, it is apparent that carbon dioxide no longer forms carbonic acid below a pH of 6, therefore highlighting the need to add a base or buffer to the solution to maintain a basic solution.

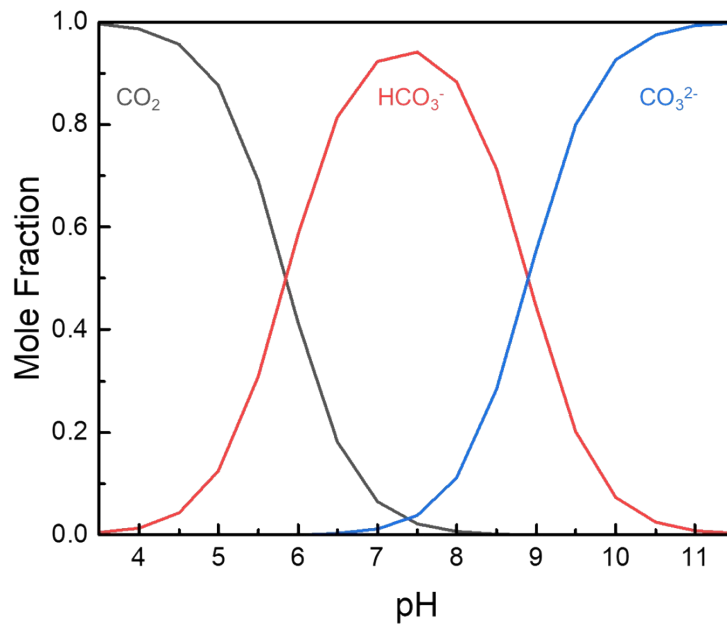


Figure S4. Speciation of carbon dioxide when dissolved in water as a function of solution pH

1.3. Carbon Negativity

The ASPEN/HYSYS model was developed to model both the supercritical water oxidation (SCWO) and mineralization aspects of the hydrothermal mineralization (HTM) process.

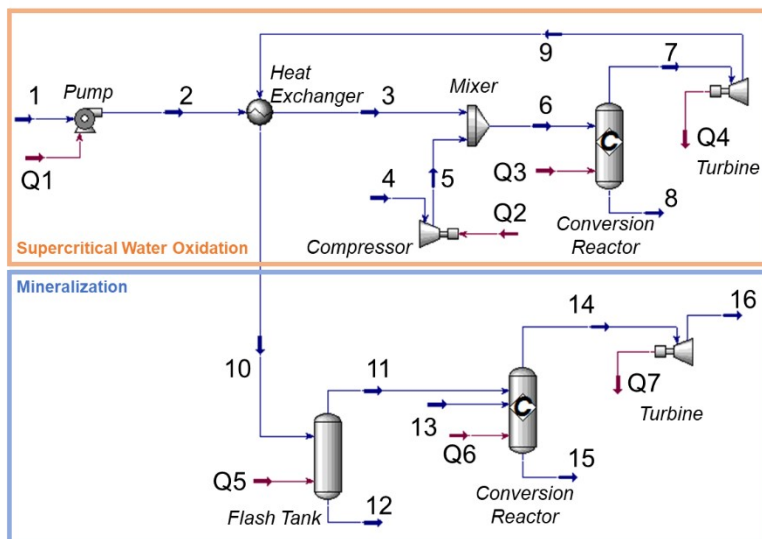


Figure S5. ASPEN/HYSYS model developed to understand the mass and energy balances with the hydrothermal mineralization process

Table S3. Mass and energy balance for 20 wt% solids loading with O:C = 3

	1	2	3	4	5	6	7	8	9	10	11	12	13	14	15	16
<i>Vapour Fraction</i>	0.00	0.00	0.00	1.00	1.00	1.00	0.00	1.00	1.00	0.80	0.00	1.00	0.00	0.00	1.00	1.00
<i>Temperature, [°C]</i>	20.00	22.45	295.20	20.00	1328.94	535.98	450.00	450.00	366.63	245.69	40.00	40.00	40.00	40.00	40.00	-154.14
<i>Pressure [atm]</i>	1.00	272.00	272.00	1.00	272.00	272.00	272.00	272.00	145.00	145.00	145.00	145.00	158.20	145.00	145.00	1.00
<i>Molar Flow [kgmole/h]</i>	9.57	9.57	9.57	12.74	12.74	22.31	0.00	22.72	22.72	22.72	10.68	12.04	4.02	4.83	11.23	11.23
<i>Mass Flow [kg/h]</i>	189.00	189.00	189.00	364.71	364.71	553.71	0.00	553.71	553.71	553.71	198.15	355.55	117.40	152.96	320.03	320.03
<i>Liquid Volume Flow [m³/h]</i>	0.20	0.20	0.20	0.42	0.42	0.62	0.00	0.63	0.63	0.63	0.20	0.42	0.08	0.10	0.38	0.38
$x_{Ca(OH)_2}$	0.00	0.00	0.00	0.00	0.00	0.00	0.00	0.00	0.00	0.00	0.00	0.00	0.20	0.00	0.00	0.00
x_{CaCO_3}	0.00	0.00	0.00	0.00	0.00	0.00	0.00	0.00	0.00	0.00	0.00	0.00	0.00	0.17	0.00	0.00
x_{O_2}	0.00	0.00	0.00	0.21	0.21	0.12	0.06	0.06	0.06	0.06	0.00	0.12	0.00	0.00	0.13	0.13
x_{N_2}	0.00	0.00	0.00	0.77	0.77	0.44	0.43	0.43	0.43	0.43	0.00	0.81	0.00	0.00	0.87	0.87
$x_{H_2O_2}$	0.88	0.88	0.88	0.02	0.02	0.39	0.45	0.45	0.45	0.45	0.96	0.00	0.80	0.83	0.00	0.00
x_{CO_2}	0.00	0.00	0.00	0.00	0.00	0.00	0.04	0.04	0.04	0.04	0.00	0.07	0.00	0.00	0.00	0.00
x_{CH_3OH}	0.12	0.12	0.12	0.00	0.00	0.05	0.02	0.02	0.02	0.02	0.03	0.00	0.00	0.00	0.00	0.00

The energy balance around the HTM system shows that hydrothermal liquefaction ($O:C = 0$) requires an input of energy. Unlike the other scenarios, the HTL condition requires no air compression (**Yellow**), but the reaction is largely endothermic (**Green**) and thus energy must be put into the system to maintain the supercritical temperature. When oxidant is introduced to the system, the reaction shifts towards combustion and drives the process to an energy negative process.

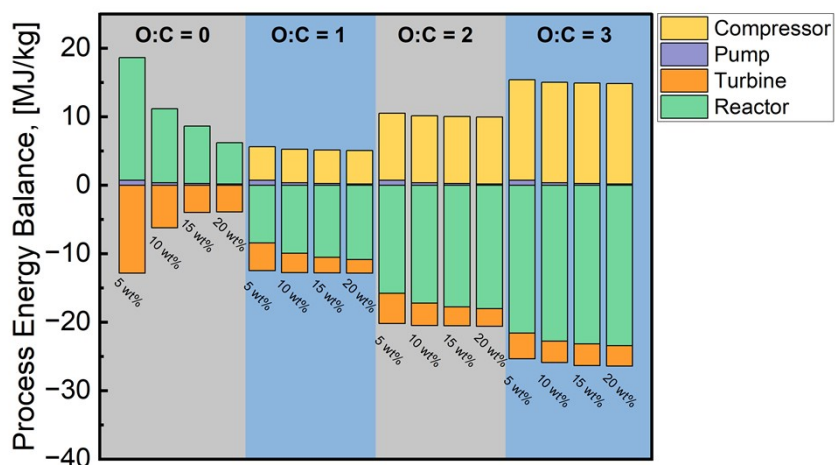


Figure S6. Breakdown of energy balance as a function of unit operations within the HTM process

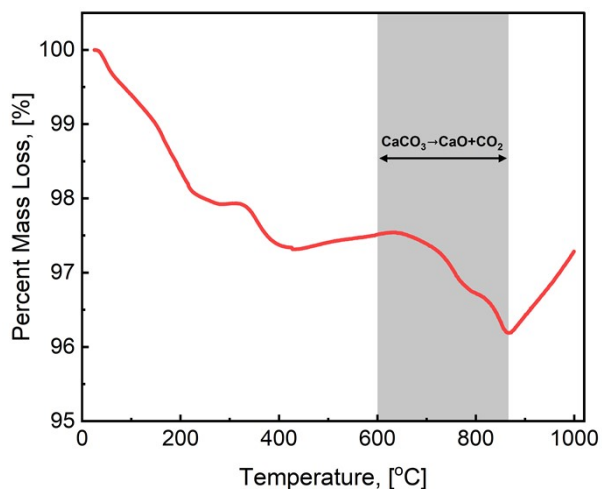


Figure S7. Thermogravimetric analysis of a produced ACM sample

1.4. Material analysis

Since the ACM was prepared with calcium chloride (CaCl_2) as a calcium source, it is important to acknowledge the presence of residual Cl^- in the material. It is important to note that CaCl_2 is a source of calcium, validating that any calcium salt can be used.

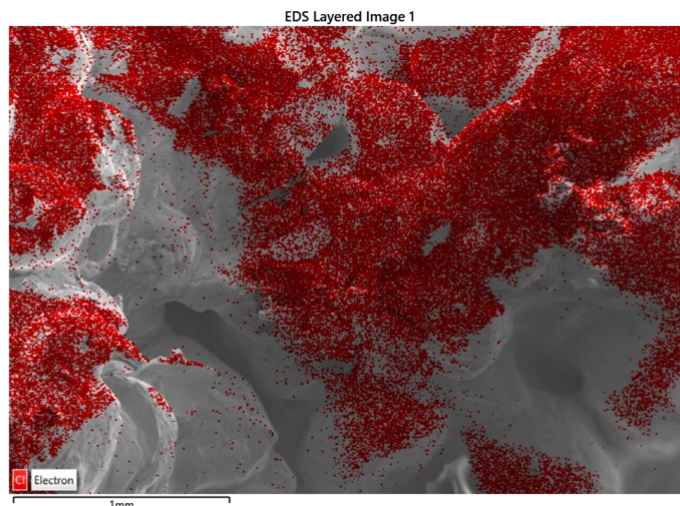


Figure S8. SEM-EDS analysis of residual chlorine within the ACM material

2. Methods

2.1.1. Supercritical Water Oxidation of Food Waste

Using a Parr 4756A high-temperature, high-pressure reactor the food waste, oxidant and water were reacted at 400-450°C. After the 1-hour reaction time, the vessel was rapidly cooled to 40°C at which point the headspace was vented into a 2 L graduated cylinder through a three-way valve to measure the gas volume via liquid displacement. Once the gas has equilibrated, gas was withdrawn from the graduated cylinder through a septum attachment which prevented mixing and contamination of the produced gas and the external air. Using a gas-tight syringe, 1 mL of the reaction gas was injected onto the GC to be measured via TCD analysis.

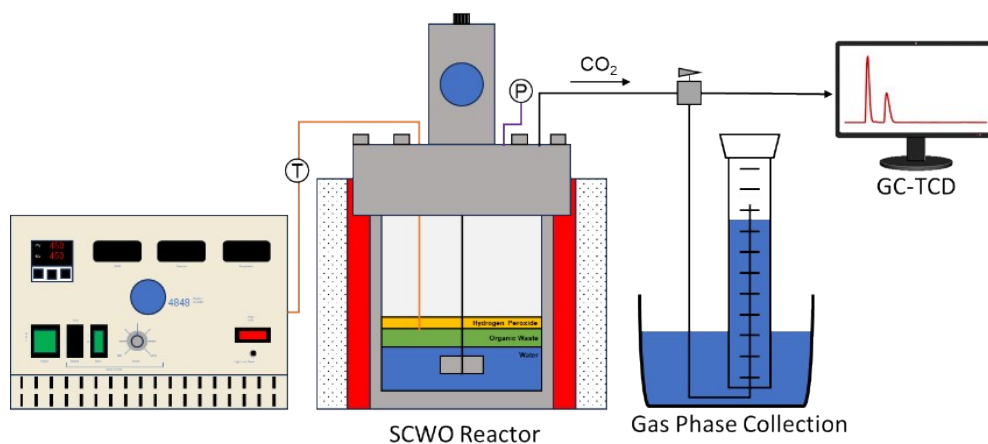


Figure S9. Reaction and analysis diagram



Figure S10. Parr reactor vessel used for SCWO experiments

The GC analysis was calibrated through individual injections of nitrogen and carbon dioxide of varying volumes. The peak area of each injection was correlated with their respective volume. For nitrogen, beyond 0.4 mL there appeared to be a different response that required a 2-part calibration. It should be noted that O_2 and N_2 have a similar elution time within the GC-TCD and were considered to be a single gas volume during the headspace analyses.

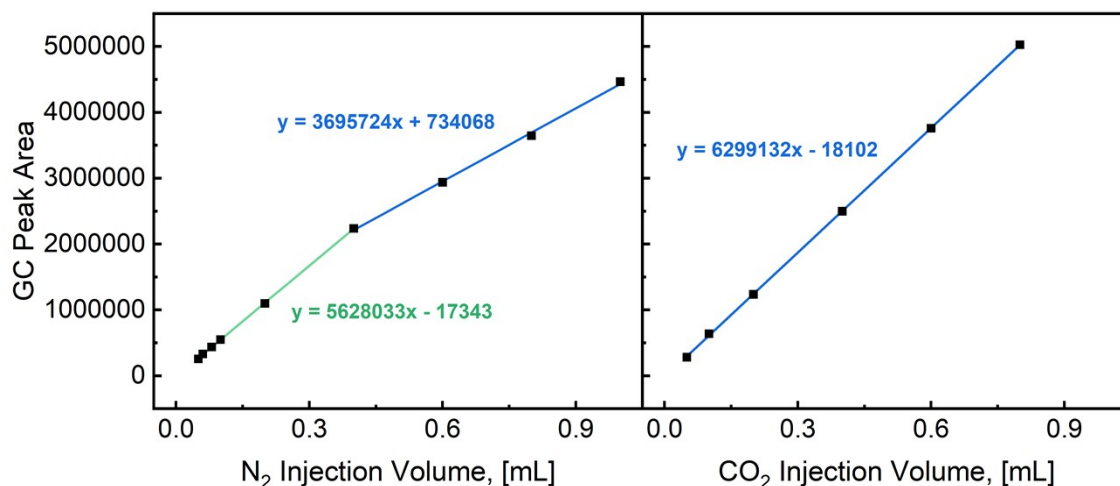


Figure S11. GC-TCD calibrations of nitrogen (LEFT) and carbon dioxide (RIGHT). Nitrogen required a two-part calibration to capture the TCD response of low injection volumes and high injection volumes

2.1.2. Modeling the SCWO mechanism

The lumped kinetic model for this system was simplified to be the conversion of food waste directly to carbon dioxide, with a representative rate expression:

$$r_{CO_2} = A_{CO_2} \exp\left(-\frac{Ea_{FW}}{RT}\right) [FW]^n [O_2]^m$$

All concentrations were determined by dividing molar quantities by the total reactor volume (250 mL), since the reaction takes place in the supercritical regime all reactants and products were assumed to be well mixed. To determine the concentration of food waste ($[FW]$) a representative molecular formula was needed to convert weight to moles. Previous SCWO studies have shown that nitrogen will form N_2 or N_2O whereas sulfur will form inorganic salts.⁹ Additionally, since nitrogen and sulfur were less than 10% of the food waste by mass the waste was assumed to be composed solely of carbon, hydrogen, and oxygen. The normalized weight percents were calculated to be:

Table S4. Normalized elemental compositions for dehydrated food waste

Element	Weight Percent (%)
C	56.19
H	8.07
O	35.74

After obtaining the weight percents, each species was converted to moles to determine the molar ratio.

$$100 \text{ g FW} \left(0.5619 \frac{\text{g C}}{\text{g FW}} \right) \left(\frac{1 \text{ mol C}}{12 \text{ g C}} \right) = 4.6825 \text{ mol C}$$

$$100 \text{ g FW} \left(0.0807 \frac{\text{g H}}{\text{g FW}} \right) \left(\frac{1 \text{ mol H}}{1 \text{ g H}} \right) = 8.07 \text{ mol H}$$

$$100 \text{ g FW} \left(0.3574 \frac{\text{g O}}{\text{g FW}} \right) \left(\frac{1 \text{ mol O}}{16 \text{ g O}} \right) = 2.2338 \text{ mol O}$$

All species were normalized to oxygen since it has the smallest number of moles, giving the following mole ratios:

Table S5. Elemental molar ratios within dehydrated food waste

Element	Mole Ratio (mol/mol O)
C	2.1
H	3.6
O	1

Lastly, all ratios were multiplied by a factor of 10 to eliminate partial molar ratios, giving the final molecular formula of $C_{21}H_{36}O_{10}$ with a molecular weight of 448 g/mol.

The model was fit in two steps, the first fitting isothermal conversion were modeled to obtain $k(450^\circ\text{C})$, n , and m . For this model, the value of n was constrained to be a first order reaction with respect to food waste, based on previous literature.¹⁰ Parameter values were solved by using MATLAB's *lsqnonlin* non-linear solver to minimize the error between the final predicted CO_2 concentration and experimental CO_2 concentrations. The ordinary differential equation (ODE) system was solved using *ode45*. To ensure the identified parameters produce the global minimum solution, MATLAB's *globalsearch* function was used to vary initial parameter guesses to find the optimal parameter solutions. Figure S12 shows the optimal solution for $[k:0.0011 \text{ } n:1 \text{ } m:0.6534]$.

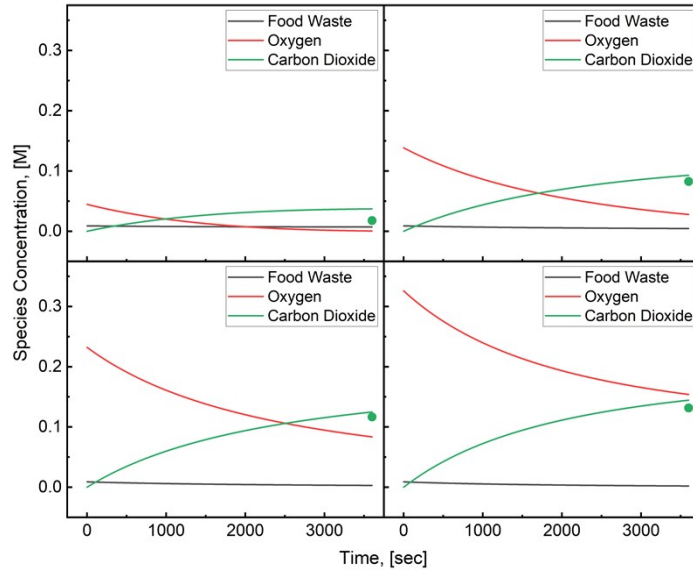


Figure S12. ODE solutions for optimized k , n , and m for isothermal conversion at 450°C. As the oxidant loading is increased there is a resultant increase in CO₂ concentration.

The second model fit was fitting conversion at O:C = 3 from 400 – 450°C to solve for the apparent activation energy (Ea) of food waste combustion under hydrothermal conditions. Since the rate coefficient can be expanded to:

$$k = A \exp\left(\frac{-Ea}{RT}\right)$$

The rate expression being solved in MATLAB was transformed to:

$$r_{CO_2} = \frac{0.0011}{\exp\left(\frac{-Ea_{FW}}{R \cdot 723K}\right)} \exp\left(\frac{-Ea_{FW}}{RT}\right) [FW]^1 [O_2]^{0.6534}$$

The apparent activation energy was solved using the same workflow and suite of MATLAB functions as the first model fit.

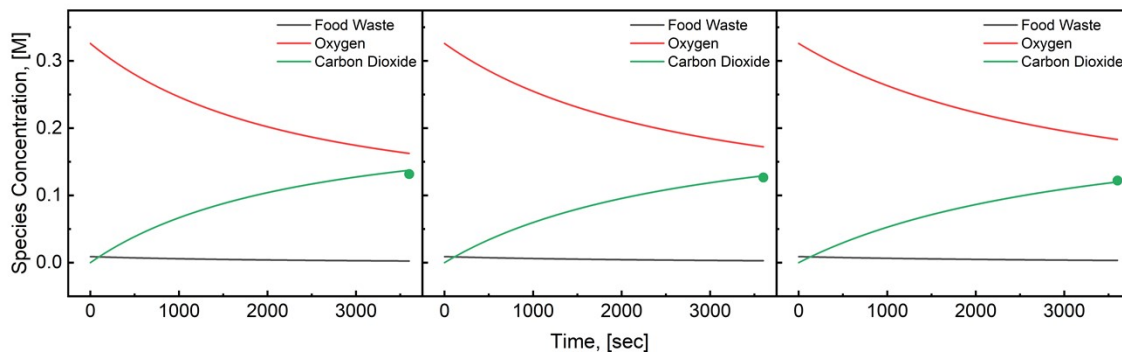


Figure S13. The conversion is found to decrease subtly as temperature decreases (LEFT to RIGHT)

Lastly, confidence intervals for each fitting parameter using *nlparci* which required residuals and Jacobian matrices from the *lsqnonlin* function as well as the fitted parameters, giving the final fitted equation of:

$$r_{CO_2} = 10^{-1.13 \pm 2.28} \exp\left(\frac{-25.3 \pm 29.4}{RT}\right) [FW][O_2]^{0.6534 \pm 6.5375}$$

2.2. CaCO₃ yield analysis and kinetic parameters

X-ray diffraction was chosen as the primary method of measuring the conversion of Ca(OH)₂ to CaCO₃. This method was possible because the primary mineralization product was calcite which had enough distinct characteristic peaks that were different from Ca(OH)₂ that they could be correlated to solids loading within the sample. Powder mixtures of various solids loading of Ca(OH)₂ and CaCO₃ were mixed well and analyzed on the XRD (Fig. S14, LEFT). While the largest calcite characteristic peak is at 29°, the peak between 37.6 and 41.1° was chosen due to the linear correlation between peak area and solids loading (Fig. S14, RIGHT). The peak area was found by taking the raw XRD data and using MATLAB's *cumtrapz* function to calculate the cumulative area beneath the curve.

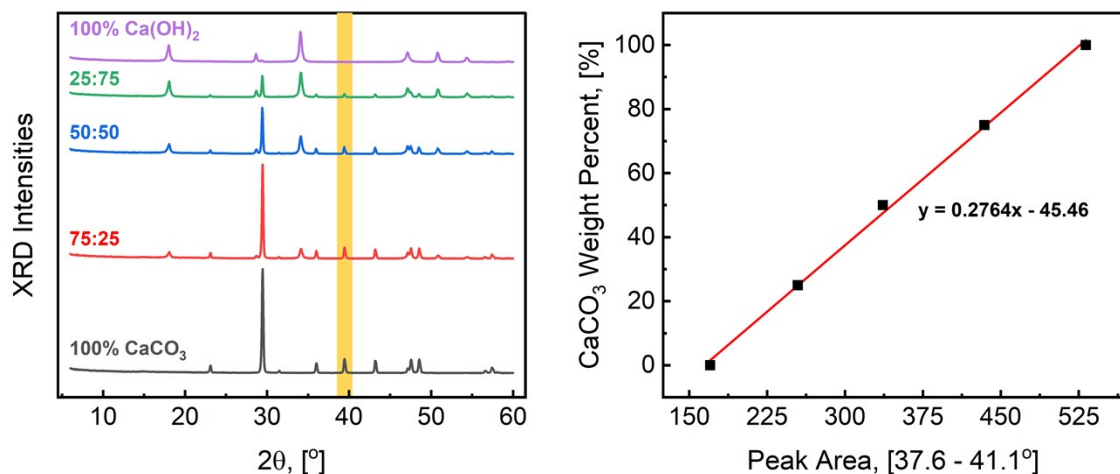


Figure S14. (LEFT) XRD analysis of powder mixtures of pure CaCO_3 and Ca(OH)_2 at different solid loadings. (RIGHT) Correlation of peak area between 37.6 – 41.1 for each solid loading.

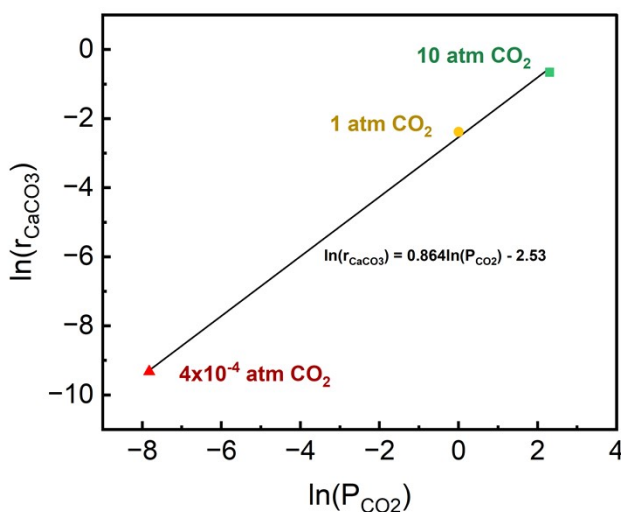
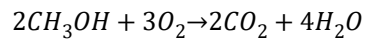


Figure S15. Plot of $\ln(r)$ vs $\ln(P)$

2.3. Process Model Development

The SCWO system was modeled in Aspen HYSYS v14. To simplify the model, methanol (CH_3OH) was used to represent the food waste because methanol is a predefined compound within Aspen HYSYS, has a similar carbon weight percent (38 wt%) compared to food waste (52 wt%) and has a comparable energy content (24 MJ/kg).¹¹ Due to the high-pressure within the reaction systems there was no concern of the methanol creating a biphasic mixture with water. The process was assigned the Peng-Robinson fluid

package to accurately represent the conversion reactions. Using more ideal fluid packages produce a bottoms product in the SCWO reactor when all products should leave from the top stream as a supercritical fluid. The reactions defined in this model is the combustion of methanol:



For the reaction, various conversions were assigned based on the experimental SCWO findings at 450°C

and O:C = 0 – 3.

2.4. Development of lifecycle analysis

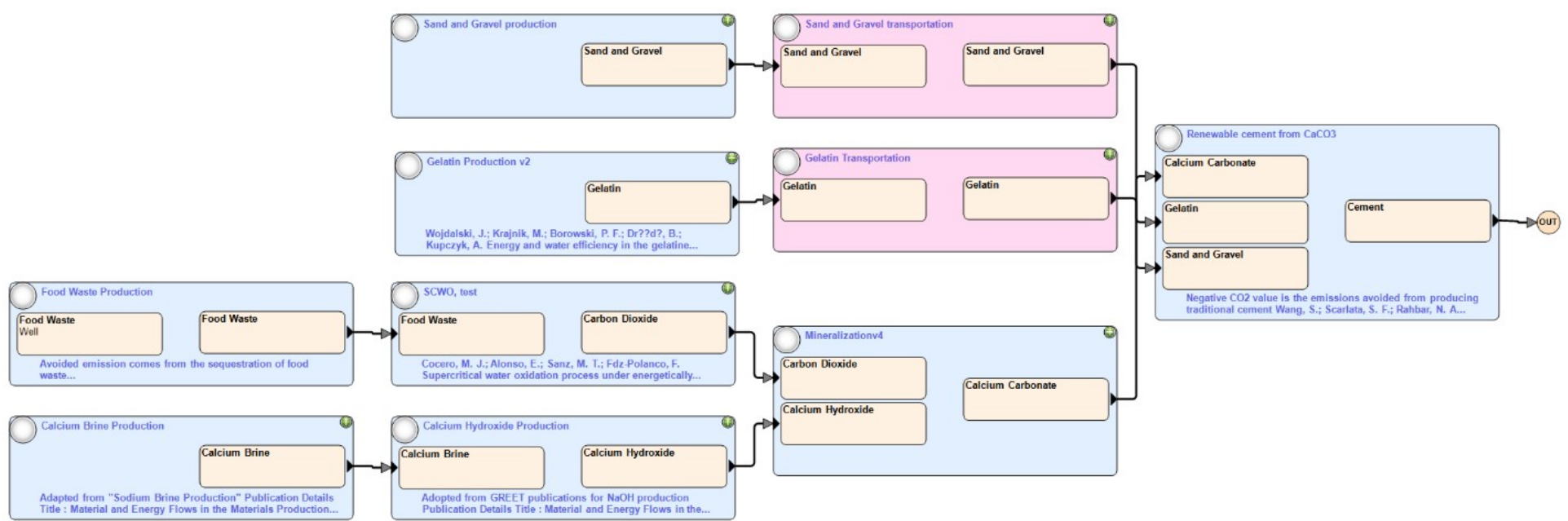


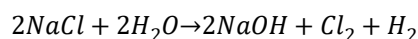
Figure S16. Process flow diagram for waste-to-concrete process in GREET

The supercritical water oxidation block within the model can be tuned to vary conversion, solids loading, O:C ratio, and if the process is consuming or producing energy.

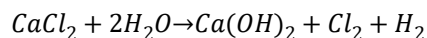
Drag and Drop Inputs below		Drag and Drop Main Output below	
Food Waste	Quantity: 100 ton Source: Output of a previous proce	Carbon Dioxide	Quantity: 144.3750 ton Losses
Water	Quantity: 400 ton Source: Primary Resource		
Oxygen	Quantity: 450 ton Source: Single Pathway Pathway: Production of ox	Drag and Drop other Outputs Below	
		Electricity	Quantity: 760221.03 MJ

Figure S17. Process inputs and outputs for SCWO in GREET

The mineralization process assumes full conversion as was seen in Fig. 2f. The calcium hydroxide production pathways were self-defined but based on calculations for the chloroalkyl process of sodium hydroxide. The chloroalkyl process for sodium hydroxide is defined as:



Argonne National Laboratory (ANL) defines that 1 ton of Cl_2 requires 7.6 mmBtu where 20% of the energy is supplied by natural gas and the remaining energy is supplied through electricity.¹²⁻¹⁴ If a sodium brine is replaced with CaCl_2 then the reaction becomes:



Based on stoichiometry, we can calculate the energy demand to be 7,693.4 MJ/ton Ca(OH)_2 maintaining the 80/20 split between electricity and natural gas. To produce 1 ton of Ca(OH)_2 requires 1.5 tons of CaCl_2 which is 3.5 tons of CaCl_2 brine, considering the solubility of CaCl_2 in solution is 42.7 weight percent. ANL additionally provides that the chloroalkyl process of NaOH requires 3773.9 gal of water per ton NaOH produced. This means that the production of Ca(OH)_2 requires 4016.13 gal/ton Ca(OH)_2 .

Drag and Drop Inputs below		Drag and Drop Main Output below
Electricity Quantity: 6154.7200 MJ Source: Single Pathway Pathway: Pathway: Distributed - U.S.	Natural Gas Quantity: 1538.6800 MJ Source: Single Pathway Pathway: Pathway: NA NG from Sha	Calcium Hydroxide Quantity: 1 ton Losses
Water Quantity: 4016.3000 gal Source: Primary Resource	Calcium Brine Quantity: 3155 kg Source: Output of a previous proce	Drag and Drop other Outputs Below

Figure S18. Process inputs and outputs for calcium hydroxide production

Figure S19 accounts for the sourcing of calcium brines which were adapted from GREET's existing calculations for NaCl.

Drag and Drop Inputs below		Drag and Drop Main Output below
Natural Gas Quantity: 0.6770 mmBtu Source: Single Pathway Pathway: Pathway: NA NG from Sha	Utility/Industrial Boiler - Natural Gas 50 % Small Industrial Boiler <10 mmBtu/hr - Natural Gas 50 %	Calcium Brine Quantity: 1 ton Losses
Electricity Quantity: 0.2220 mmBtu Source: Single Pathway Pathway: Pathway: Distributed - U.S.		Drag and Drop other Outputs Below
Residual Oil Quantity: 0.1110 mmBtu Source: Single Pathway Pathway: Pathway: Residual Oil (Pet	Industrial Boiler - Residual Oil 100 %	

Figure S19. Process inputs and outputs for calcium brine production

Lastly, the production of the alternative concrete mortar follows the recipe laid out by Wang et al. in the production of enzymatic construction materials as well as the experiments carried out in this study. The concrete mixture called for 3 g of sand, 0.08 g of gelatin, and 0.26 g of $\text{CaCl}_2 \cdot 2\text{H}_2\text{O}$.




Drag and Drop Inputs below		Drag and Drop Main Output below
<div><div> Calcium Carbonate</div><div>Quantity <input type="text" value="85 mg"/></div><div>Source <input type="text" value="Output of a previous proce"/></div></div>	<div><div> Gelatin</div><div>Quantity <input type="text" value="90 mg"/></div><div>Source <input type="text" value="Output of a previous proce"/></div></div>	<div><div> Cement</div><div>Quantity <input type="text" value="3 g"/></div><div><input type="text" value="Losses"/></div></div>
		Drag and Drop other Outputs Below

Figure S20. Process inputs and outputs for ACM production

3. References

- 1 *National Overview: Facts and Figures on Materials, Wastes and Recycling*, <<https://www.epa.gov/facts-and-figures-about-materials-waste-and-recycling/national-overview-facts-and-figures-materials>> (2022).
- 2 Kamran, A., Chaudhry, M. N. & Batool, S. A. Effects of socio-economic status and seasonal variation on municipal solid waste composition: a baseline study for future planning and development. *Environmental Sciences Europe* **27**, 16, doi:10.1186/s12302-015-0050-9 (2015).
- 3 Hla, S. S. & Roberts, D. Characterisation of chemical composition and energy content of green waste and municipal solid waste from Greater Brisbane, Australia. *Waste Management* **41**, 12-19, doi:<https://doi.org/10.1016/j.wasman.2015.03.039> (2015).
- 4 Fujiwara, T., Inoue, R., Ohtawa, T. & Tsunoda, M. Liquid-Chromatographic Methods for Carboxylic Acids in Biological Samples. *Molecules* **25**, doi:10.3390/molecules25214883 (2020).
- 5 Stair, R. Ultraviolet Absorption Spectra of Seven Substituted Benzenes.
- 6 Sager, E. E., Schooley, M. R., Carr, A. S. & Acree, S. Ultraviolet spectra and dissociation constants of p-hydroxybenzoic acid, methyl, ethyl, n-butyl, and benzyl p-hydroxybenzoate and potassium p-phenolsulfonate. *J. Res. Nat. Bur. Stand.* **35**, 521-538 (1945).
- 7 Lisov, A., Vrublevskaya, V., Lisova, Z., Leontievsky, A. & Morenkov, O. A 2,5-Dihydroxybenzoic Acid–Gelatin Conjugate: The Synthesis, Antiviral Activity and Mechanism of Antiviral Action Against Two Alpha herpesviruses. *Viruses* **7**, 5343-5360 (2015).
- 8 Mojica Prieto, F. J. & Millero, F. J. The values of pK₁ + pK₂ for the dissociation of carbonic acid in seawater. *Geochimica et Cosmochimica Acta* **66**, 2529-2540, doi:[https://doi.org/10.1016/S0016-7037\(02\)00855-4](https://doi.org/10.1016/S0016-7037(02)00855-4) (2002).
- 9 Marrone, P. A. Supercritical water oxidation—Current status of full-scale commercial activity for waste destruction. *The Journal of Supercritical Fluids* **79**, 283-288, doi:<https://doi.org/10.1016/j.supflu.2012.12.020> (2013).
- 10 Chen, S., Qu, X., Zhang, R. & Bi, J. Destruction of representative submarine food waste using supercritical water oxidation. *Environmental Science and Pollution Research* **22**, 4527-4533, doi:10.1007/s11356-014-3689-7 (2015).
- 11 Linstrom, P. Vol. NIST Standard Reference Database Number 69 (NIST Office of Data and Informatics, 2021).
- 12 Dunn, J. B., Gaines, L., Barnes, M., Sullivan, J. L. & Wang, M. Material and energy flows in the materials production, assembly, and end-of-life stages of the automotive lithium-ion battery life cycle. (Argonne National Lab.(ANL), Argonne, IL (United States), 2014).
- 13 Sullivan, J. & Gaines, L. A review of battery life-cycle analysis: state of knowledge and critical needs. (2010).
- 14 Lampert, D. J. *et al.* Development of a life cycle inventory of water consumption associated with the production of transportation fuels. (Argonne National Lab.(ANL), Argonne, IL (United States), 2015).